ACS OMEGA

http://pubs.acs.org/journal/acsodf

Article

# Failure Mechanism of the Corrugated Medium under Simulated Cold Chain Logistics

Hongxia Su, Chongxing Huang,* Cuicui Li, Yuan Zhao, Dantong Zheng, and Qingshan Duan

Cite This: *ACS Omega* 2023, 8, 23673−23682

Read Online

ACCESS | Metrics & More | Article Recommendations

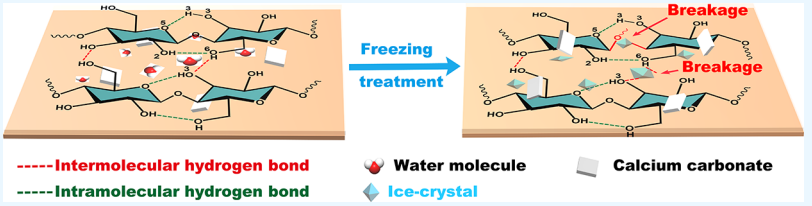


**ABSTRACT:** It is necessary to develop corrugated medium food packaging, which is suitable for highly humid environments, to meet the demands of cold chain logistics. In this paper, we investigated the influence of the transverse ring crush index of different environmental factors of corrugated medium and the failure mechanisms during cold chain transportation. After freeze−thaw treatment of corrugated medium, XRD and DP showed a decrease in crystallinity and polymerization of 3.47 and 7.83%, respectively. Also, the FT-IR spectra of the paper showed that the number of intermolecular hydrogen bonds decreased by about 3.00% after freezing. SEM and XRD showed $CaCO_3$ precipitation on the paper surface and a 26.01% increase in pore size. This study would be beneficial in further expanding the applications of cellulose-based paperboard cold chain transportation.

## 1. INTRODUCTION

During the 2030 Sustainable Development Goals implementation, the increasing global concern of food wastage and its significant environmental, economic, and social impacts have been highlighted.[1] According to the Food and Agriculture Organization of the United Nations, 1.6 billion tons of food are wasted globally each year, of which the edible portion amounts to 1.3 billion tons.[2] To address this problem of food wastage, cold chain transportation provides an effective solution.[3] According to the 2021−2027 global and Chinese packaging market status and future development, there are expanding scale and growing demand for the global cold chain logistics industry. However, although packaging for cold chain transportation is an important research area, there are limited studies available on paper packaging materials.

Globally, corrugated cardboard plays an essential role in storing, transporting, and protecting products, including agricultural products, electronics, and everyday items such as fresh fruits, vegetables, and flowers. For example, corrugated cardboard is commonly utilized in the export handling of pome fruits (such as apples and pears) in the South African fruit industry.[4] In China, foam and corrugated box packaging are typically used for cold chain logistics, in which polystyrene usage accounts for >80% of the packaging materials. However, the low degradability of polymer materials poses an urgent concern for environmental pollution. Thus, paper and paper-based packaging materials are the most crucial breakthrough in cold chain packaging.[5]

Because of their powerful environmental friendliness,[6,7] excellent processing performance,[8,9] and great potential for modification,[10,11] paper and paper-based packaging materials have a very broad application prospect in the cold chain transport packaging field. However, for cold chain logistics applications, paper and paper-based packaging materials exhibit a decrease in their mechanical properties in the return temperature owing to the considerable changes in the humidity and temperature.[12] In detail, as corrugated cartons for frozen foods are usually stored in cold storage for long durations at −18 to −24 °C, they experience significant temperature changes during transportation. During the rewarming process, their water content increases, which reduces the compressive strength of the corrugated cartons,[13] thereby damaging them and affecting the quality of their contents. Before this, there has not been a related system to conduct an in-depth research on it. Therefore, it is necessary to conduct a systematic and detailed study of the failure mechanism of corrugated paper during cold chain transportation, which will help to develop a corrugated paper suitable for highly humid environments and applicable for cold chain food packaging.

**Received:** March 15, 2023
**Accepted:** June 15, 2023
**Published:** June 26, 2023

The mechanical strength of fiber materials is determined by factors such as fiber stiffness, inter-fiber bond strength, material density, etc.[14] Different fiber sources are the main factors affecting fiber stiffness. The choice of raw materials should be considered upon paper-based packaging for cold chain logistics. Fadiji et al.[15,16] found that the main factors affecting the strength of corrugated paperboard packaging are the manufacturing process and cold chain environment. Jarupan et al.[17] prepared molded pulp trays from fibers extracted from oil palm leaves for protective packaging and studied their mechanical properties at high humidity [90% relative humidity (RH)] and low temperature (12 °C). Studies on the performance of paper and paper-based packaging materials have mainly focused on the structure changes at different temperatures and humidity to analyze the inter-fiber bond strength and material density. Sundholm and Tahvanainen[18−20] conducted a series of accelerated aging experiments on paper at constant humidity and different temperatures to evaluate the temperature dependence of mechanical properties. These high RH conditions result in large moisture contents[12] in the corrugated fiberboard, which adversely affects board strength, due to water molecules breaking hydrogen bonds (HBs) in the cellulose fiber;[21] meanwhile, infrared spectroscopy can be used to evaluate the changes in the HB structure. Lojewski et al.[22] investigated the changes in the HB network during hydro desorption and sorption cycles at different humidities and temperatures by infrared spectroscopy. Previous studies have shown the calculation methods of simulating cold chain packaging for transport.[23] However, the performance of paper-based packaging materials at low temperatures is yet to be systematically explored. Furthermore, the failure mechanism of paper-based packaging materials at low temperatures has not yet been revealed.

The compressive strength of the corrugated carton is closely related to the edge compression strength of the corrugated board, which is associated with the ring crush strength of the corrugated medium.[24] Hence, a high transverse ring crush (TRC) strength is required for corrugated media. In this paper, a corrugated medium was subjected to different cold chain environmental conditions to study the changes in its TRC index and to reveal its failure mechanism. The changes in the surface composition, chemical structure, crystallinity, and microstructure of the corrugated medium before and after the freezing were also investigated. The present study provides relevant findings in the application of paper-based packaging materials in cold chain transportation.

## 2. MATERIALS AND METHODS

**2.1. Materials.** The corrugated medium paper was purchased from Liaoning Xingdong Science and Technology Co., Ltd. It was composed of 46% softwood pulp, 47% hardwood pulp, and 7% straw pulp with a grammage of 120 g/m$^2$ and a thickness of 170 $\mu$m. The content of $CaCO_3$ in the paper was 23.14%. The paper sheets were stored at 23 ± 1 °C and 50 ± 2% RH for 48 h before the test. The water content in the samples stored under such conditions is approximately 7 wt %.[22,25]

**2.2. Corrugated Medium under a Simulated Cold Chain Environment.** Single-factor experiments of the water content, freezing temperature, freezing time, and freeze−thaw cycles were conducted. The final experimental conditions were determined based on the minimum TRC resistance. Hereafter, the corrugated medium, frozen corrugated medium, and corrugated medium paper with the lowest TRC index are referred to as $S_C$, $S_F$, and $S_D$, respectively.

Water was applied to the corrugated base paper by spraying. Here, water content refers to the ratio of the water weight absorbed by the paper to the corrugated medium paper weight. The moist paper was placed into a sealed bag to preserve moisture.

To explore the influence of the number of freeze−thaw cycles on the TRC strength of corrugated base paper, the freeze−thaw cycle was defined. A freeze−thaw cycle refers to the process of freezing a corrugated medium in a low-temperature refrigerator (−30 °C) for 30 min and subsequently placing it in a chamber with a constant temperature of 23 ± 1 °C and a RH of 50% for 30 min.

**2.3. Determination of the TRC Index.** Ring crush tests were performed to determine the ring crush resistance of the paper strip formed into a ring with a standardized length and width. The length and width of the paper strip were 152 and 12.7 mm, respectively. It was subsequently rolled to form a cylinder with a radius of 24.64 mm, which was inserted in a circular groove with a depth of 6.35 mm. A compression load was applied to the edge of the paper strip, whose bottom half was supported by the holder. GB/T2679.8 standard was used for measuring the ring crush resistance, and the TRC index was calculated using the following formula:

$$r = R/W \tag{1}$$

where $r$, $R$, and $W$ are the TRC index (N m/g), ring crush resistance (N/m), and grammage (g/m$^2$), respectively.

**2.4. Field Emission−Scanning Electron Microscopy (FE−SEM).** FE−SEM (SU8020, Hitachi, Tokyo, Japan) was employed to visualize the morphological changes of the corrugated base paper before and after freezing at a voltage of 10 kV. Prior to imaging, the samples were gold coated using a sputter coater.

**2.5. Brunauer−Emmett−Teller (BET) Surface Analysis.** The BET method with $N_2$ adsorption/desorption was used for the surface analysis of the corrugated base paper. The structural characteristics of the pores at 77 K were obtained from the $N_2$ adsorption−desorption isotherms using a fully automatic multi-station surface area and porosity analyzer (ASAP 2460, Micromeritics, Norcross, Georgia, USA). Degassing was performed at 90 °C for 12 h before the experiment. The Barrett−Joyner−Halenda (BJH) model is a generally accepted model for pore size distribution calculation developed based on Kelvin's theory of capillary coalescence. The pore size distribution was determined using the BJH method by assuming that the pore type is a cylindrical pore and applying Kelvin's equation through simple geometric calculations.

**2.6. X-ray Diffraction (XRD).** XRD (SmartLab, Rigaku, Osaka, Japan) under the operating conditions of Cu K$\alpha$ radiation at 40 kV and 35 mA was employed for the crystallinity analysis. The scanning range and speed were set to 5−40° and 5 °/min, respectively. The crystallinity index (CrI) was calculated as follows:[26,27]

$$\mathrm{CrI}\ (\%) = (I_{002} - I_{\mathrm{am}})/I_{002} \times 100\% \tag{2}$$

where $I_{002}$ is the maximum intensity of the crystalline peak with $2\theta$ = 22−23° and $I_{\mathrm{am}}$ is the minimum intensity of the non-crystalline region with $2\theta$ = 18−19°.

**2.7. Degree of Polymerization (DP).** According to GB/T 1548−2016, the degree of polymerization (DP) of corrugated


https://doi.org/10.1021/acsomega.3c01668
ACS Omega 2023, 8, 23673−23682

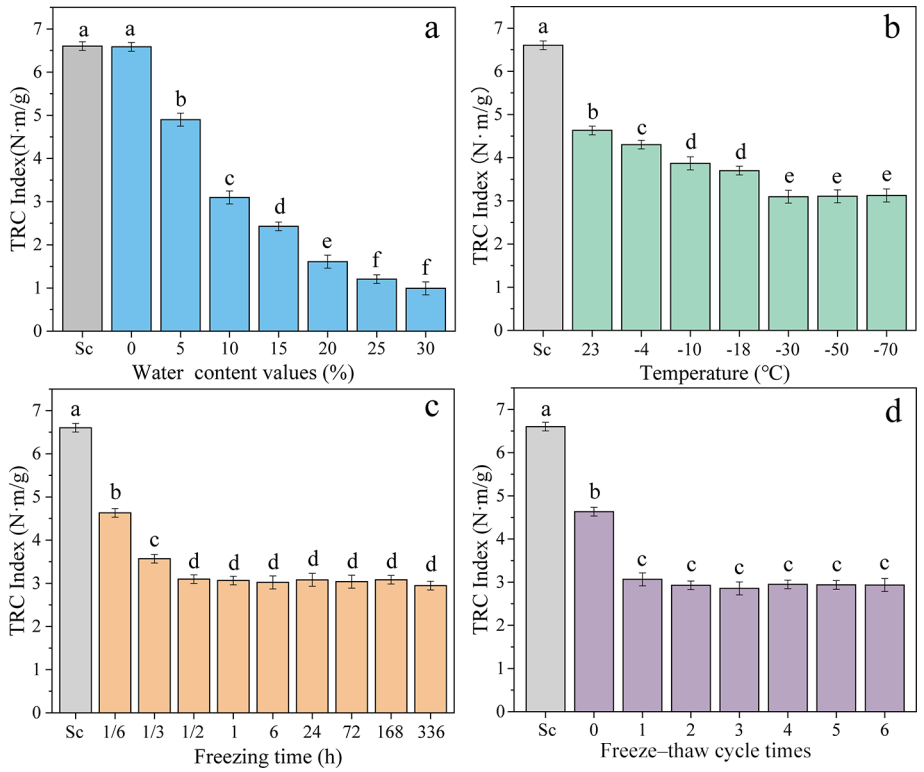


**Figure 1.** Effect of the (a) water content (freezing temperature of −30 °C, freezing time of 12 h, and one freeze−thaw cycle), (b) temperature (moisture content of 10%, freezing time of 12 h, and one freeze−thaw cycle), (c) freezing time (moisture content of 10%, freezing temperature of −30 °C, and one freeze−thaw cycle), and (d) number of freeze−thaw cycles (moisture content of 10%, freezing temperature of −30 °C, and freezing time of 30 min) on the TRC index of the corrugated medium.

base paper is measured by the pulp dissolved in copper ethylenediamine solution viscosity method. DP of cellulose was calculated by the following formula:

$$DP^{0.905} = 0.75 \times [954 \times \log(X) - 325] \quad (3)$$

where $X$ is the fiber viscosity measured according to the $T$ 230 om-99 TAPPI standard method.

**2.8. Attenuated Total Reflection−Fourier Transform Infrared (ATR−FTIR) Spectroscopy.** FTIR (Nicolet iS50 FTIR spectrometer, ThermoFisher Scientific, Waltham, Massachusetts, USA) spectroscopy was used to qualitatively observe the chemical structure of the corrugated base paper before and after freezing. The spectra were recorded in the scanning range of 4000−400 $cm^{-1}$ with a scanning resolution of 4 $cm^{-1}$ and 64 scans per sample. Spectral deconvolution was performed using PeakFit software with the Gaussian distribution function.[28] The correlation value of the deconvolution fitting was $r^2 \geq 0.99$.

**2.9. X-ray Photoelectron Spectroscopy (XPS).** XPS (ESCALAB 250Xi, ThermoFisher Scientific, Waltham, Massachusetts, USA) was employed for the chemical characterization of the elemental composition and functional groups. Two positions on the corrugated medium surface were selected for testing. The collected data were analyzed using Thermo Scientific Advantage software (ThermoFisher Scientific, USA).

**2.10. Thermogravimetric (TG) Analysis.** The samples were added to a crucible to analyze their thermal stability using a TG analyzer (TA55, TA instruments, New Castle, Delaware, USA) with a heating rate of 10 °C/min, a temperature range of 50−600 °C, and a nitrogen purge of 20 mL/min.

**2.11. Statistical Analysis.** The data were analyzed using the analysis of variance (ANOVA) of the SPSS 16.0 program (SPSS Inc., Chicago, IL, USA). The statistical correlations were evaluated using Pearson's correlation coefficients. $p < 0.05$ was considered statistically significant. The figures were drawn using the Origin 8 program (OriginLab Corp., Northampton, MA, USA).

## 3. RESULTS AND DISCUSSION

**3.1. Conditions for the Lowest TRC Index.** Here, water content refers to the ratio of the water weight absorbed by the paper to the corrugated medium weight at 23 ± 1 °C and 50 ± 2% RH. Figure 1a depicts the effects of different water content values on the TRC index of the corrugated medium. The water content values were set to 5, 10, 15, 20, 25, and 30% at a cold chain temperature of −30 °C, a freezing time of 12 h, and one freeze−thaw cycle; the samples are defined as $S_{WX}$, where $X$ is the water content in mass%. $S_F$ and $S_C$ exhibit similar TRC values, which gradually decrease with the increase in water content. The TRC index of $S_{W10}$ is 3.10 N m/g (53.11% lower than that of $S_C$), which could not satisfy the standard for corrugating media (GB/T 13023−2008). Meanwhile, the TRC index of $S_{W30}$ is 84.94% lower than that of $S_F$. The decrease in the TRC index is attributed to the hygroscopic nature of paper, indicating its sensitivity to moisture. The exposure of icy cartons to high temperatures and RHs during storage, handling, and transportation results in the condensation of the water vapor close to the carton, which is absorbed by the carton and subsequently affects its strength.[29] During the continuous transport of cartons under a cold chain environment after rewetting, the absorbed water freezes and forms ice


https://doi.org/10.1021/acsomega.3c01668
ACS Omega 2023, 8, 23673−23682

crystals. The volume of the water expands by approximately 9% below the freezing point.[30,31] The expansion of the condensates exhibits a positive correlation to the volume of the absorbed water,[32] which damages the fiber structure, thereby adversely affecting the mechanical properties of the carton.

Figure 1b shows the effects of the cold chain temperature (23, −4, −10, −18, −30, −50, and −70 °C) on the TRC index of the corrugated medium with a water content of 10%, a freezing time of 12 h, and one freeze−thaw cycle; the samples are labeled as $S_{TX}$, where $X$ is the cold chain temperature. The TRC index of the corrugated medium gradually decreases with decreasing temperature. The TRC index for $S_{T\text{-}30}$ decreased by 53.11% compared to that of $S_C$, whereas that of $S_{T\text{-}70}$ decreased by 32.54% compared to that of $S_{T23}$. The TRC index reached its minimum at −30 °C, and the continued decrease in temperature did not affect it. This result is ascribed to the effect of temperature on the ice crystal size. This is because a higher amount of water is absorbed during the melting phase at a lower freezing temperature after moisture absorption, leading to the formation of more and larger crystals in the paper.[33] This damages the material structure and reduces the strength of the corrugated medium. This damages the nature of the fibers themselves to some extent and affects the HBs and other forces generated within the fibers, thus reducing the strength of the corrugated medium. Meanwhile, the water that remains liquid at higher temperatures (23 °C), as the freezing temperature decreases (≤ −4 °C), such as that in the small capillary pores, gradually begins to freeze until it is completely frozen (≤ −20 °C).[34] The volume of water expands as it turns into ice, and this increased swelling force breaks the HBs between the fibers, which weakens the fiber bonds, thereby decreasing the TRC index.

The effects of the freezing time on the TRC index of the corrugated medium are illustrated in Figure 1c. The freezing times were set to 0, 1/6, 1/3, 1/2, 1, 6, 24, 72, 168, and 336 h with 10% water content, a freezing temperature of −30 °C, and one freeze−thaw cycle; the samples are defined as $S_{tX}$, where $X$ is the freezing time (h). The TRC index of the corrugated medium gradually decreases as the freezing time increases. The TRC index of $S_{t1/2}$ decreased by 52.53% relative to that of $S_C$ and 32.42% relative to that of $S_{t0}$. As the freezing time further increased, the TRC index remained constant. The decrease in the TRC index for $S_{t1/2}$ is due to the uneven freezing of the paper fibers with a relatively short freezing time. When the freezing time is too short, the center of its fibers has not yet reached the temperature at which water freezes, and therefore, some liquid water is still present in the fibers. However, with the increase in freezing time, the amount and volume of ice crystals formed increase within the paper, thereby damaging the nature of the fibers themselves and breaking the bonds between the fibers and consequently resulting in a detrimental effect on the TRC strength of the corrugated medium.

A freeze−thaw cycle refers to the process of freezing a corrugated medium in a low-temperature refrigerator (−30 °C) for 30 min and subsequently placing it in a chamber with a constant temperature of 23 ± 1 °C and RH of 50% for 30 min. Figure 1d depicts the effects of the number of freeze−thaw cycles on the TRC index of the corrugated medium. The number of freeze−thaw cycles was set to 0, 1, 2, 3, 4, 5, and 6, with a water content of 10%, a freezing temperature of −30 °C, and a freezing time of 30 min; the samples are defined as $S_{CX}$, where $X$ is the number of freeze−thaw cycles. The TRC index of the corrugated medium gradually decreases as the number of freeze−thaw cycles increases. The TRC index of $S_{C3}$ decreased by 56.76% relative to that of $S_C$, whereas that of $S_{C6}$ decreased by 39.46% relative to that of $S_{C0}$. The effect of the number of freeze−thaw cycles on the TRC index can be attributed to the formation and melting of ice crystals. During each freeze−thaw treatment, the ice crystals form at low temperatures, and small ice crystals melt with a gradual increase in temperature, whereby the melted ice crystals regroup on the slightly larger ice crystals to form larger ice crystals as the temperature is decreased again.[35,36] Thus, the water recrystallization in the fibers led to the wetting and swelling of the fibers, thereby increasing their structural damages[34] and causing a decrease in the TRC index of the corrugated medium.

Therefore, the experimental conditions for the lowest TRC index of 2.86 N m/g of the corrugated medium, which does not meet the standard carton strength, are as follows: a water content of 10%, a freezing temperature of 30 °C, a freezing time of 30 min, and three freeze−thaw cycles.

**3.2. FE−SEM Analysis.** Figure 2 illustrates the surface morphology of $S_C$, $S_F$, and $S_D$ obtained by FE−SEM. Paper is a

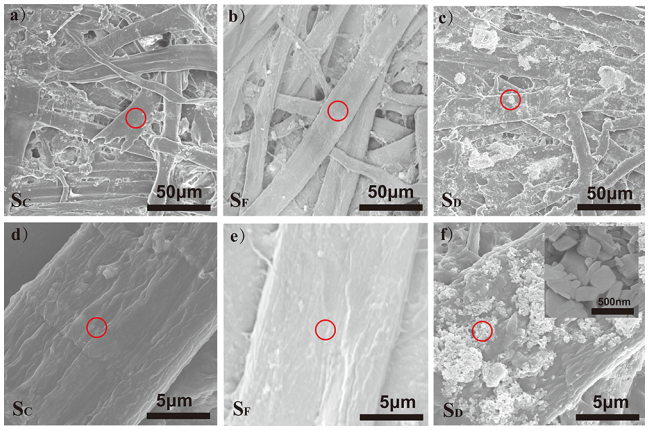


**Figure 2.** FE−SEM images of the (a, d) corrugated medium ($S_C$), (b, e) frozen corrugated medium ($S_F$), and (c, f) corrugated medium with the lowest TRC index ($S_D$).

disordered porous material with a three-dimensional structure composed of fibers and inorganic mineral fillers. Based on the macroscopical observations, there are no abnormalities on the $S_C$ and $S_F$ surfaces, whereas a large number of white clusters is observed on the $S_D$ surface. The $S_C$ and $S_F$ paper surfaces exhibited a small adherence, and their fiber surfaces are relatively smooth. Meanwhile, the fiber surface of $S_D$ is attached to many granular nanomaterials with a relatively regular shape, which is the paper filler ($CaCO_3$) precipitated from the fibers.[37] Due to the large amount of precipitation of $CaCO_3$ filtered in the paper under the condition of moisture absorption and freezing, the gap between the fibers increased, and the ability to bond between the fibers decreased. The paper became looser and more porous, which led to a decline in the physical strength of the paper.

**3.3. BET Analysis.** The specific surface areas of the samples were determined using BET analysis, and the pore diameter distribution of the samples was determined using the BJH model. The BET surface areas of the different samples were determined from the $N_2$ adsorption isotherm data at 77 K, as shown in Table 1. The adsorption−desorption isotherms of $N_2$ for $S_C$, $S_F$, and $S_D$ are depicted in Figure 3a−c, and BJH


https://doi.org/10.1021/acsomega.3c01668
ACS Omega 2023, 8, 23673−23682

**Table 1. BET Surface Area and BJH Adsorption Average Pore Diameter of the Paper Samples Determined from the $N_2$ Adsorption Isotherm[a]**

| paper sample | BET specific surface area ($m^2/g$) | BJH adsorption average pore diameter (nm) |
|---|---|---|
| $S_C$ | 0.6904 ± 0.074 | 39.33 ± 1.37 |
| $S_F$ | 0.5777 ± 0.043 | 40.65 ± 1.98 |
| $S_D$ | 0.3623 ± 0.056 | 49.56 ± 1.85 |

[a] $S_C$, corrugated medium; $S_F$, frozen corrugated medium; $S_D$, corrugated medium with the lowest TRC index.

adsorption d$V$/d$D$ pore volume is depicted in Figure 3d. According to the IUPAC classification, the isotherms are found to be type IV with H3 hysteresis loops,[38] indicating the mesoporous structure of the corrugated medium. The surfaces of the fiber-based materials exhibit a non-uniform pore size distribution owing to the non-uniform fiber arrangement.[39] Compared with that of $S_C$, the specific surface area of $S_D$ decreased by 47.52%, whereas the average pore size increased by 26.01%. This is attributed to the water absorbed by the fibers, whose volume expanded after freezing,[32] thereby increasing the voids between the fibers and the average pore size of the sample.

**3.4. XRD Analysis.** Crystallinity is an important parameter for polymer characterization. A high crystallinity indicates superior mechanical properties of the material.[40] Figure 4 presents the crystallinity of $S_C$, $S_F$, and $S_D$ obtained through XRD. The signals at 29, 36, 39, 47.5, and 48.5° are diffraction peaks of the calcite-type $CaCO_3$ fillers.[41] The peaks at 15.4, 16.6, and 22.5° correspond to the crystalline regions of the cellulose fibers.[42] The crystallinity of samples $S_C$, $S_F$, and $S_D$ calculated using eq 2 is 79.32, 78.94, and 75.85%, respectively.

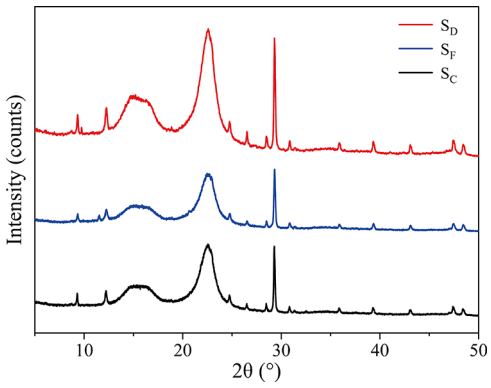


**Figure 4.** XRD pattern of the corrugated medium ($S_C$), frozen corrugated medium ($S_F$), and corrugated medium with the lowest TRC index ($S_D$).

The results demonstrate that one-time freezing has minimal effects on the crystallinity of the corrugated medium, whereas refreezing after rewetting results in considerable changes in their amorphous-to-crystalline ratio. This phenomenon is attributed to the breakage of the HBs and crystalline regions of the fibers when water is frozen, thereby reducing the crystallinity and strength of the cellulose fibers.[43] This observation is consistent with previous findings, which suggested that the lower strength of the HBs between adjacent cellulose chains loosens the cellulose structure and lowers the crystallinity of a material, thereby decreasing its mechanical properties.[41,44]

**3.5. DP Analysis.** DP directly affects the mechanical strength of the paper samples,[45,46] as reflected by the structural changes in the fibers. The DP for $S_C$, $S_F$, and $S_D$ is 448, 441,

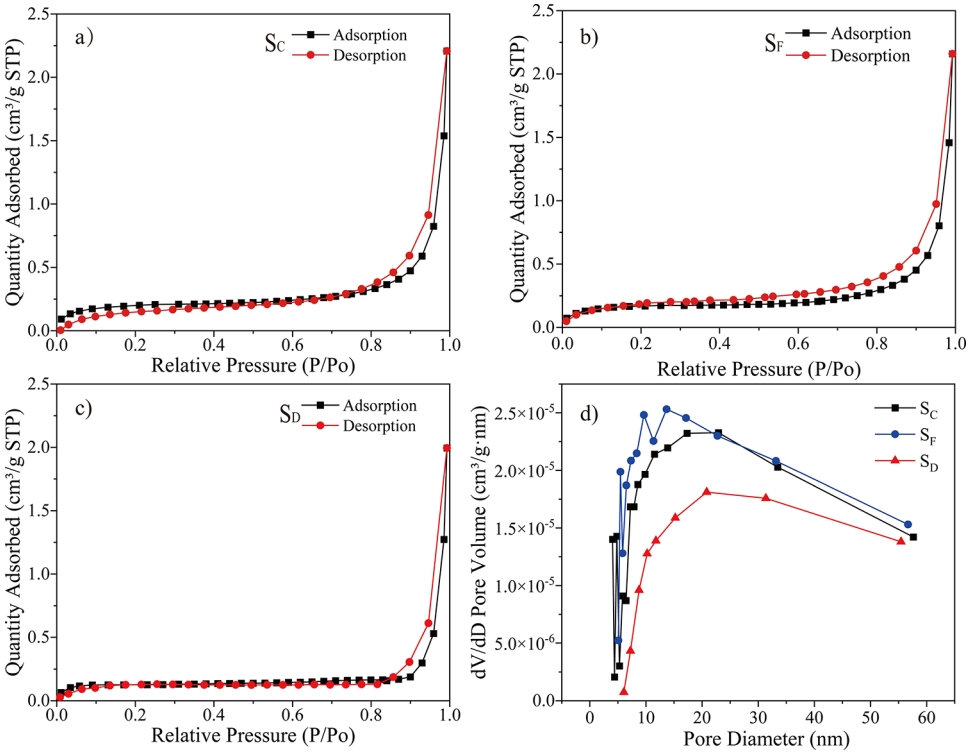


**Figure 3.** $N_2$ adsorption−desorption isotherms for the (a) corrugated medium ($S_C$), (b) frozen corrugated medium ($S_F$), and (c) corrugated medium with the lowest TRC index ($S_D$) at $T$ = 77 K. (d) Pore diameter distribution of $S_C$, $S_F$, and $S_D$ from the BJH model.



https://doi.org/10.1021/acsomega.3c01668
ACS Omega 2023, 8, 23673−23682

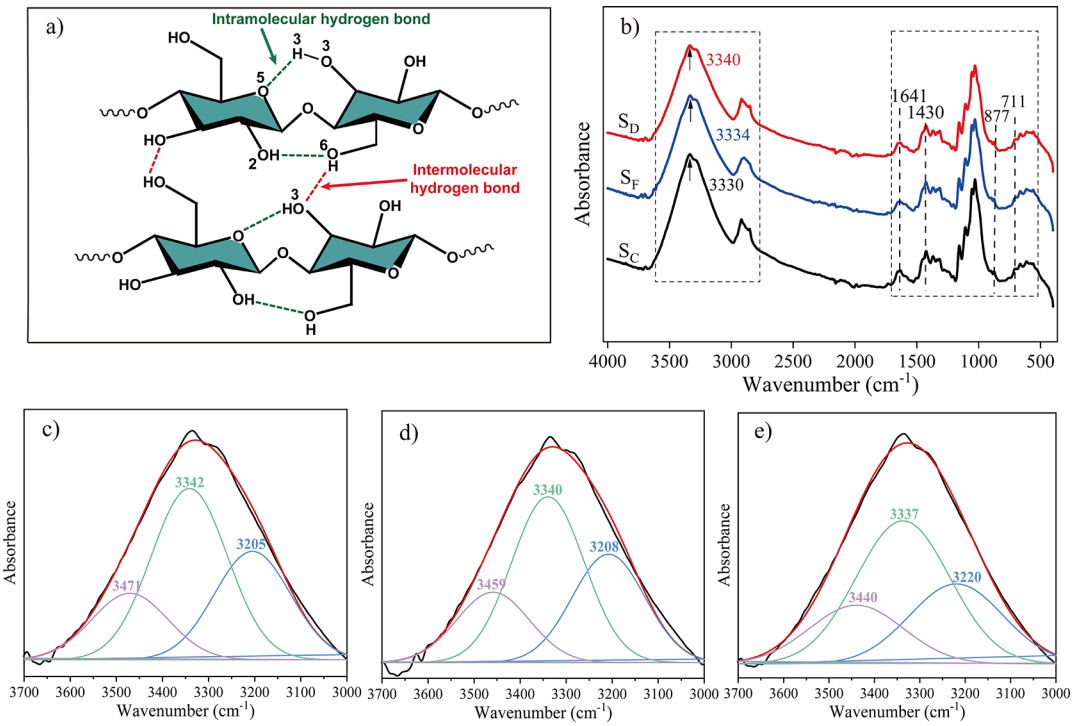


**Figure 5.** (a) Hydrogen bonding in the corrugated medium. (b) Spectra of the corrugated medium ($S_C$), frozen corrugated medium ($S_F$), and corrugated medium with the lowest TRC index ($S_D$); (c–e) deconvoluted spectra of the HB region of $S_C$, $S_F$, and $S_D$, respectively.

and 400, respectively. The DP reduction is attributed to the shortened molecular length as the cellulose chains are broken by freezing, which weakens the strength of the paper. Similar results were obtained by Fang et al.[47] who investigated the pivotal role of cellulose DP in increasing the mechanical strength of nano-cellulose films.

**3.6. ATR–FTIR Analysis.** FTIR spectroscopy is an appropriate technique widely employed to characterize the chemical groups on the surface of fibers. Figure 5 presents the typical FTIR spectra of $S_C$, $S_F$, and $S_D$. Two main characteristic regions are observed in the spectra of all samples, the high- (3500–2800 cm$^{-1}$) and low- (1700–500 cm$^{-1}$) wavenumber regions, which agrees with those of a previous report.[48] The peaks at 1430, 877, and 711 cm$^{-1}$ are attributed to $CaCO_3$,[49] which is consistent with the XRD and FE–SEM results. The strong (saturated) absorption peak at 1430 cm$^{-1}$ is ascribed to the asymmetric stretching vibration of the C–O bond. There are no new absorption peaks observed for $S_F$ and $S_D$ compared to the FTIR spectra of $S_C$. The results indicate that the environmental changes in the corrugated medium during cold chain transportation did not produce new functional groups.

The broad spectral band in the 3700–3000 cm$^{-1}$ region corresponds to the stretching vibration of the hydrogen-bonded OH groups in the cellulose molecule, demonstrating the hydrophilic tendency of the fiber.[48] Specifically, the absorption peak of the HB of $S_D$ shifted to a higher wavenumber compared with that of $S_C$ (approximately 3300 cm$^{-1}$), indicating the looser HBs of $S_D$. The intramolecular HBs ($HB_{intra}$) of O2H···O(6) and O(3)H···O(5) and intermolecular HBs ($HB_{inter}$) of O(6)H···O(3) (Figure 5a)[50] are considered to contribute to the bands at 3410–3460, 3340–3375, and 3230–3310 cm$^{-1}$,[51,52] respectively, as indicated in Figure 5b.

Spectral deconvolution (Figure 5c–e) is an efficient tool to increase the analytical power of the bands indicated above in terms of the HB characterization. The quantitative results obtained after the baseline corrections are listed in Table 2.

**Table 2. Proportional Abundances of the Classes of HBs in the FTIR Spectra**[a]

| paper sample | type of HB | wavenumber (cm$^{-1}$) | abundancy (%) | curve fitting ($r^2$) |
|---|---|---|---|---|
| $S_C$ | O(2)H···O(6) | 3471 | 19.21 | 0.996 |
| | O(3)H···O(5) | 3342 | 49.47 | |
| | O(6)H···O(3) | 3205 | 31.32 | |
| $S_F$ | O(2)H···O(6) | 3459 | 20.44 | 0.993 |
| | O(3)H···O(5) | 3340 | 48.11 | |
| | O(6)H···O(3) | 3208 | 31.44 | |
| $S_D$ | O(2)H···O(6) | 3440 | 20.83 | 0.995 |
| | O(3)H···O(5) | 3337 | 50.78 | |
| | O(6)H···O(3) | 3220 | 28.39 | |

[a] $S_C$, corrugated medium; $S_F$, frozen corrugated medium; $S_D$, corrugated medium with the lowest TRC index.

The shift in the O (6)H···O(3) intermolecular bonds of $S_D$ appeared at higher wavenumbers (weaker bonds)[34,53] compared with that of $S_C$, implying that the ice crystals could destroy the intermolecular HBs. Furthermore, the peak area of $S_D$ $HB_{inter}$ O (6)H···O(3) decreased by approximately 3.00%, indicating the increased distance between the cellulose chains. Moreover, the HBs between the cellulose molecules were broken by the formation of ice crystals, resulting in a decrease in the intermolecular HBs.

**3.7. XPS Analysis.** XPS was employed to record the broad spectra and high-resolution narrow spectra of the surface elements of $S_C$, $S_F$, and $S_D$ in the range 0–1350 eV. Figure 6 depicts the XPS spectra, showing C and O as the primary elements in the samples. The $S_D$ surface C content decreased from 69.19 to 61.19%, whereas the surface O and Ca content


https://doi.org/10.1021/acsomega.3c01668
ACS Omega 2023, 8, 23673–23682

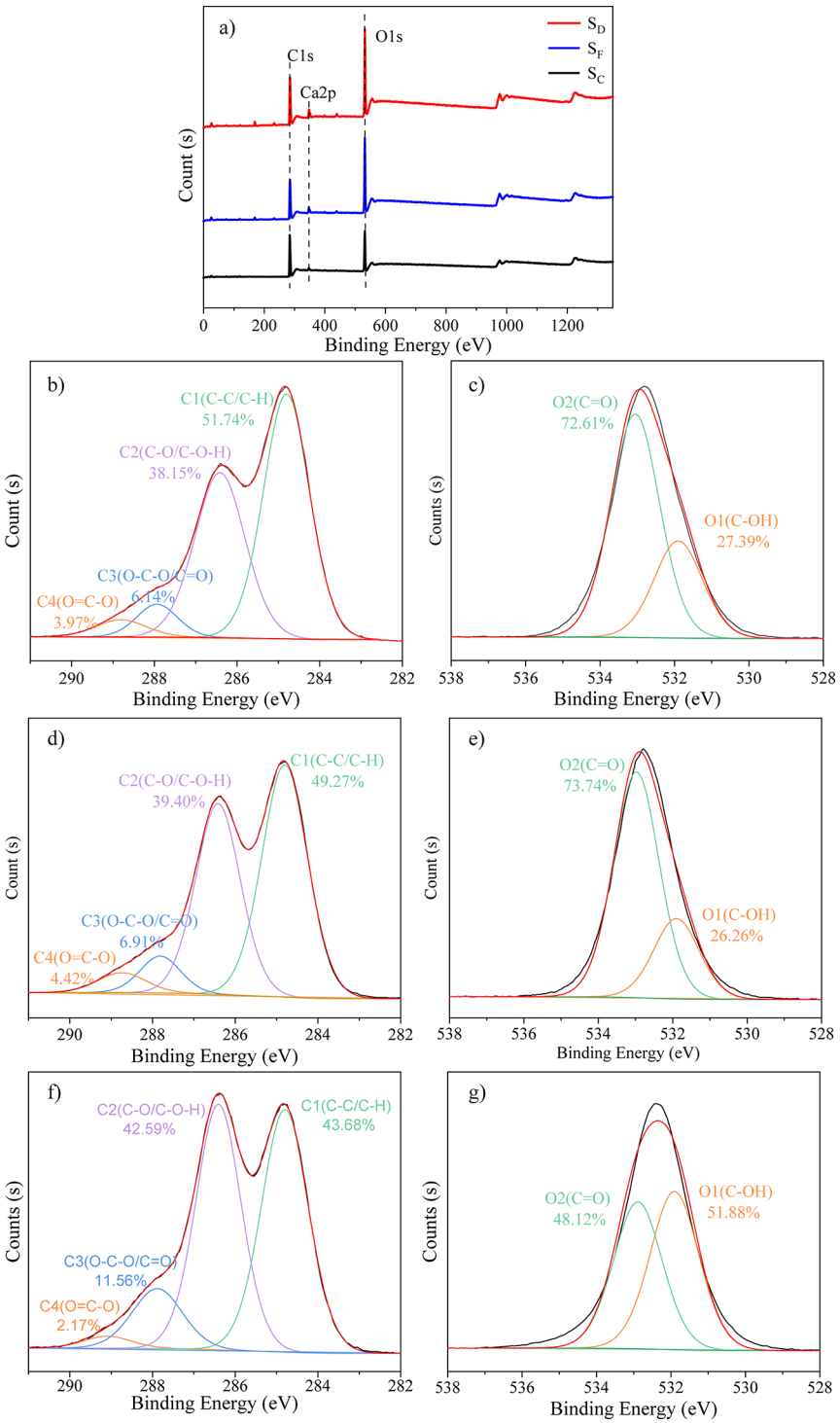


**Figure 6.** (a) XPS survey spectra of the corrugated medium ($S_C$), frozen corrugated medium ($S_F$), and corrugated medium with the lowest TRC index ($S_D$). (b) C 1s and (c) O 1s for $S_C$. (d) C 1s and (e) O 1s for $S_F$. (f) C 1s and (g) O 1s for $S_D$.

increased from 30.28 to 37.07% and 0.53 to 1.74%, respectively, compared with that of $S_C$, which is consistent with the previous FE-SEM results. The change in the C and O contents may be attributed to the breakage of bonds between the fibers by the ice crystals.

The deconvolution of C 1s presented four functional groups, namely, C−C/C−H (284.8 eV), C−O/C−O−H (286.3 eV), O−C−O/C═O (287.9 eV), and O═C−O (288.9 eV) at different binding energies (BEs).[54,55] Additionally, the deconvolution of O 1s revealed two functional groups at different BEs, namely, C−OH (231.9 eV) and C═O (232.9 eV).[56] These results demonstrate a considerable increase in C−O/C−OH after the freezing treatment. Moreover, this indicates that the C−O/C−OH/C═O groups are polysaccharides.[57] After the freeze−thaw treatment, the C−OH content increased by 24%, which can be attributed to the breakage of the intermolecular and intramolecular HBs of the paper cellulose chains, thereby exposing more OH groups.

**3.8. TG Analysis.** The TG analysis determined the thermal properties of $S_C$, $S_F$, and $S_D$. The thermal stability of the



https://doi.org/10.1021/acsomega.3c01668
ACS Omega 2023, 8, 23673−23682

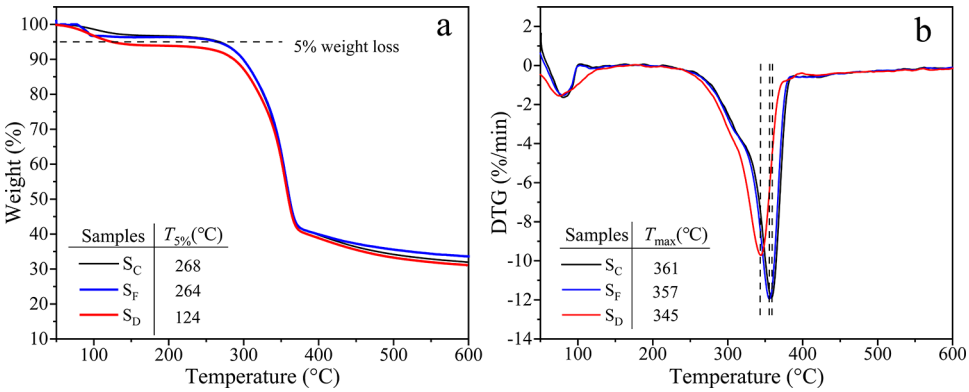


**Figure 7.** Thermal properties of the corrugated medium ($S_C$), frozen corrugated medium ($S_F$), and corrugated medium with the lowest TRC index ($S_D$): (a) TG curves and (b) differential TG curves.

polymeric materials depends on the inherent characteristics of the sample and molecular interactions between the different macromolecules.[58] Figure 7 shows the TG and derivative thermogram curves of $S_C$, $S_F$, and $S_D$. The thermogravimetric process of the corrugated medium in the $N_2$ atmosphere includes three major steps. The first stage involves a small amount of weight loss at ∼100 °C, which is related to the evaporation of the water loosely bound to the cellulose surface.[59] This loss can also be observed from the characteristic peak of the bending vibration of the intermolecular hydrogen-bonded water interaction at 1641 $cm^{-1}$ in the FTIR spectrum, which is in line with a previous study.[60] In addition, thermal degradation did not occur in this stage. The second degradation stage at 220−300 °C is attributed to the thermal depolymerization of the hemicellulose and cleavage of the glycosidic linkages of cellulose.[61,62] Finally, the last stage includes thermal degradation at 250−450 °C, which is related to the degradation of the lignin components and depolymerization of the cellulose structure. Moreover, a majority of the cellulose content is decomposed at this stage.[48]

During cold chain transportation, the $T_{5\%}$ of $S_C$, $S_F$, and $S_D$ decreased from 268 to 264 to 124 °C due to the crystallinity and polymerization of the cellulose induced by the freezing process. The thermal stability of the corrugated medium at high temperatures decreased after freeze−thaw treatment, as indicated by the decrease in $T_{max}$ (from 361 to 357 to 345 °C)[42] and residual ash content.[63] Moreover, the thermal stability of the corrugated medium greatly decreased by the freeze−thaw treatment, as confirmed by the decrease in mechanical strength.

## 4. CONCLUSIONS

This study investigated the effects of environmental factors on the TCR index of the corrugated medium during cold chain transportation. The water content, freezing temperature, freezing time, number of freeze−thaw cycles, and their effects on the properties of the corrugated medium were simulated. The experimental results revealed that the reduction in the strength of the corrugated medium was mainly attributed to three factors: first, the reduced strength of the cellulose fibers based on their crystallinity and polymerization; second, the destruction of the HBs between the fibers in the cellulose due to freezing; and third, increased voids between the cellulose fibers due to the precipitation of paper fillers.

The findings obtained in this study are beneficial to further expand the application of cellulose-based paperboard as a substrate for cold chain packaging. Based on the obtained strength degradation mechanism of the corrugated medium during cold chain transportation, modification methods can be explored to enhance the mechanical and barrier properties of the corrugated medium. Further, the findings of this study provide great insights for alleviating environmental pollution and decreasing the cost of packaging in cold chain transport through the use of paper-based packaging materials.

## AUTHOR INFORMATION


### Corresponding Author

**Chongxing Huang** − *School of Light Industry & Food Engineering, Guangxi University, Nanning 530004, China; Guangxi Key Laboratory of Clean Pulp & Papermaking and Pollution Control, Nanning 530004, China;* orcid.org/0000-0002-4368-9499; Phone: +86-771-3272256; Email: huangcx@gxu.edu.cn

### Authors

**Hongxia Su** − *School of Light Industry & Food Engineering, Guangxi University, Nanning 530004, China*

**Cuicui Li** − *School of Light Industry & Food Engineering, Guangxi University, Nanning 530004, China*

**Yuan Zhao** − *School of Light Industry & Food Engineering, Guangxi University, Nanning 530004, China;* orcid.org/0000-0002-7573-4936

**Dantong Zheng** − *School of Light Industry & Food Engineering, Guangxi University, Nanning 530004, China*

**Qingshan Duan** − *School of Light Industry & Food Engineering, Guangxi University, Nanning 530004, China*

Complete contact information is available at: https://pubs.acs.org/10.1021/acsomega.3c01668


### Author Contributions

H.S.: Conceptualization, Data curation, Writing−Original draft preparation. C.H.: Conceptualization, Writing-Reviewing and editing, Funding acquisition. C.L.: Visualization, Investigation. Y.Z.: Methodology, Software. D.Z.: Software, Validation. Q.D.: Supervision.


### Funding

The authors gratefully acknowledge partial financial support for the project from the Guangxi Natural Science Foundation of China [2019JJD120012] and Guangxi Key R & D Projects of China [2018AB45007].


### Notes

The authors declare no competing financial interest.



https://doi.org/10.1021/acsomega.3c01668
ACS Omega 2023, 8, 23673−23682

## ■ ACKNOWLEDGMENTS

The authors are grateful for the support of the large instrument platform of the Institute of Light Industry and Food Engineering, Guangxi University.

## ■ REFERENCES

(1) Liu, C.; Mao, C.; Bunditsakulchai, P.; Sasaki, S.; Hotta, Y. Food waste in Bangkok: Current situation, trends and key challenges. *Resour. Conserv. Recycl.* **2020**, *157*, No. 104779.
(2) Food and Agriculture Organization of the United Nations, Food wastage: Key facts and figures, (2020), http://www.fao.org/news/story/en/item/196402/icode/ (accessed 2020).
(3) Gwanpua, S. G.; Verboven, P.; Leducq, D.; Brown, T.; Verlinden, B. E.; Bekele, E.; Aregawi, W.; Evans, J.; Foster, A.; Duret, S.; Hoang, H. M.; van der Sluis, S.; Wissink, E.; Hendriksen, L. J. A. M.; Taoukis, P.; Gogou, E.; Stahl, V.; El Jabri, M.; Le Page, J. F.; Claussen, I.; Indergardi, E.; Nicolai, B. M.; Alvarez, G.; Geeraerd, A. H. The FRISBEE tool, a software for optimising the trade-off between food quality, energy use, and global warming impact of cold chains. *J. Food Eng.* **2015**, *148*, 2−12.
(4) Berry, T. L.; Delele, M. A.; Griessel, H.; Opara, U. L. Geometric Design Characterisation of Ventilated Multi-scale Packaging Used in the South African Pome Fruit Industry. *Ama Agr. Mech. Asia Af.* **2015**, *46*, 34−42.
(5) Chen, X.; Wang, K.; Wang, Z.; Zeng, H.; Yang, T.; Zhang, X. Highly stretchable composites based on cellulose. *Int. J. Biol. Macromol.* **2021**, *170*, 71−87.
(6) Kopacic, S.; Walzl, A.; Zankel, A.; Leitner, E.; Bauer, W. Alginate and Chitosan as a Functional Barrier for Paper-Based Packaging Materials. *Coatings* **2018**, *8*, 235.
(7) Borodulina, S.; Motamedian, H. R.; Kulachenko, A. Effect of fiber and bond strength variations on the tensile stiffness and strength of fiber networks. *Int. J. Solids Struct.* **2018**, *154*, 19−32.
(8) Nowacka, M.; Rybak, K.; Wiktor, A.; Mika, A.; Boruszewski, P.; Woch, J.; Przybysz, K.; Witrowa-Rajchert, D. The quality and safety of food contact materials - paper and cardboard coated with paraffin emulsion. *Food Control* **2018**, *93*, 183−190.
(9) Brunetti, F.; Operamolla, A.; Castro-Hermosa, S.; Lucarelli, G.; Manca, V.; Farinola, G. M.; Brown, T. M. Printed Solar Cells and Energy Storage Devices on Paper Substrates. *Adv. Funct. Mater.* **2019**, *29*, No. 1806798.
(10) Dai, L.; Xi, X.; Li, X.; Li, W.; Du, Y.; Lv, Y.; Wang, W.; Ni, Y. Self-assembled all-polysaccharide hydrogel film for versatile paper-based food packaging. *Carbohydr. Polym.* **2021**, *271*, No. 118425.
(11) Oyola-Reynoso, S.; Kihereko, D.; Chang, B. S.; Mwangi, J. N.; Halbertsma-Black, J.; Bloch, J. F.; Thuo, M. M.; Nganga, M. M. Substituting Plastic Casings with Hydrophobic (Perfluorosilane treated) paper improves Biodegradability of Low-Cost Diagnostic Devices. *Ind. Crop. Prod.* **2016**, *94*, 294−298.
(12) Parker, M. E.; Bronlund, J. E.; Mawson, A. J. Moisture sorption isotherms for paper and paperboard in food chain conditions. *Packag. Technol. Sci.* **2006**, *19*, 193−209.
(13) Berry, T. M.; Ambaw, A.; Defraeye, T.; Coetzee, C.; Opara, U. L. Moisture adsorption in palletised corrugated fibreboard cartons under shipping conditions: A CFD modelling approach. *Food Bioprod. Process.* **2019**, *114*, 43−59.
(14) Wang, Q.; Xiao, S.; Shi, S.; Cai, L. Mechanical Strength, Thermal Stability, and Hydrophobicity of Fiber Materials after Removal of Residual Lignin. *BioResources* **2018**, *13*, 71−85.
(15) Fadiji, T.; Coetzee, C.; Opara, U. L. Compression strength of ventilated corrugated paperboard packages: Numerical modelling, experimental validation and effects of vent geometric design. *Biosyst. Eng.* **2016**, *151*, 231−247.
(16) Fadiji, T.; Berry, T. M.; Coetzee, C. J.; Opara, U. L. Mechanical design and performance testing of corrugated paperboard packaging for the postharvest handling of horticultural produce. *Biosyst. Eng.* **2018**, *171*, 220−244.
(17) Jarupan, L.; Hunsa-Udom, R.; Bumbudsanpharoke, N. Potential Use of Oil Palm Fronds for Papermaking and Application as Molded Pulp Trays for Fresh Product under Simulated Cold Chain Logistics. *J. Nat. Fibers* **2022**, *19*, 2772−2784.
(18) Sundholm, F.; Tahvanainen, M. Paper conservation using aqueous solutions of calcium hydroxide/methyl cellulose 1. Preparation of the solution. *Restaurator* **2003**, *24*, 1−17.
(19) Sundholm, F.; Tahvanainen, M. Paper conservation using aqueous solutions of calcium hydroxide/methyl cellulose - 2. The influence of accelerated ageing temperature on properties of treated paper. *Restaurator* **2003**, *24*, 178−188.
(20) Sundholm, F.; Tahvanainen, M. Paper conservation using aqueous solutions of calcium hydroxide/methyl cellulose - 3. The influence on the degradation of papers. *Restaurator* **2004**, *25*, 15−25.
(21) Allaoui, S.; Aboura, Z.; Benzeggagh, M. L. Phenomena governing uni-axial tensile behaviour of paperboard and corrugated cardboard. *Compos. Struct.* **2009**, *87*, 80−92.
(22) Lojewski, T.; Miskowiec, P.; Molenda, M.; Lubanska, A.; Lojewska, J. Artificial versus natural ageing of paper. Water role in degradation mechanisms. *Appl. Phys. A* **2010**, *100*, 625−633.
(23) Wu, W. T.; Beretta, C.; Cronje, P.; Hellweg, S.; Defraeye, T. Environmental trade-offs in fresh-fruit cold chains by combining virtual cold chains with life cycle assessment. *Appl. Energy* **2019**, *254*, No. 113586.
(24) Zang, S.; Xu, L.; Sun, H. Research on Compressive Strength of High Strength Corrugated Box Based on Finite Element Analysis. *Integr. Ferroelectr.* **2021**, *213*, 21−34.
(25) Navaranjan, N.; Dickson, A.; Paltakari, J.; Ilmonen, K. Humidity effect on compressive deformation and failure of recycled and virgin layered corrugated paperboard structures. *Compos. B Eng.* **2013**, *45*, 965−971.
(26) Segal, L.; Creely, J.; Martin, A.; Conrado, C.; Segel, L.; Conrad, C.; Creely, J.; Conrad, C. An empirical method for estimating the degree of crystallinity of native cellulose using the X-ray diffractometer. *Text. Res. J.* **1959**, *29*, 786−794.
(27) Hajji, L.; Boukir, A.; Assouik, J.; Pessanha, S.; Figueirinhas, J. L.; Carvalho, M. L. Artificial aging paper to assess long-term effects of conservative treatment. Monitoring by infrared spectroscopy (ATR-FTIR), X-ray diffraction (XRD), and energy dispersive X-ray fluorescence (EDXRF). *Microchem. J.* **2016**, *124*, 646−656.
(28) Popescu, C. M.; Popescu, M. C.; Singurel, G.; Vasile, C.; Argyropoulos, D. S.; Willfor, S. Spectral characterization of eucalyptus wood. *Appl. Spectrosc.* **2007**, *61*, 1168−1177.
(29) Pathare, P. B.; Berry, T. M.; Opara, U. L. Changes in moisture content and compression strength during storage of ventilated corrugated packaging used for handling apples. *Packag. Res.* **2016**, *1*, 1−6.
(30) Vigoureux, D.; Vigoureux, J. M. How can freezing water burst pipes and containers? *Eur. J. Phys.* **2018**, *39*, No. 045808.
(31) Jin, J.; Han, L.; Cao, M.; Li, Y.; Qi, Y.; Cong, Q. Volume expansion rule of water droplets during freezing process. *J. Jilin Univ.* **2016**, *46*, 1546−1551.
(32) Zhao, Y.; Guo, Q.; Lin, T.; Cheng, P. A review of recent literature on icing phenomena: Transport mechanisms, their modulations and controls. *Int. J. Heat Mass Transfer* **2020**, *159*, No. 120074.
(33) Zhu, Z.; Zhou, Q.; Sun, D.-W. Measuring and controlling ice crystallization in frozen foods: A review of recent developments. *Trends Food Sci. Technol.* **2019**, *90*, 13−25.
(34) Zhu, H.; Ma, Q.; Sheng, J.; Yang, R. Freeze-thaw repetition as an auxiliary method to promote efficient separation of hemicellulose from poplar. *Green Chem.* **2020**, *22*, 942−949.
(35) Leducq, D.; Ndoye, F. T.; Alvarez, G. Phase change material for the thermal protection of ice cream during storage and transportation. *Int. J. Refrig.* **2015**, *52*, 133−139.
(36) Ndoye, F. T.; Alvarez, G. Characterization of ice recrystallization in ice cream during storage using the focused beam reflectance measurement. *J. Food Eng.* **2015**, *148*, 24−34.


https://doi.org/10.1021/acsomega.3c01668
*ACS Omega* 2023, 8, 23673−23682

(37) Peter, A.; Cozmuta, L. M.; Nicula, C.; Cozmuta, A. M.; Apjok, R.; Talasman, C. M.; Drazic, G.; Penas, A.; Jesus Calahorro, A.; Nzekoue, F. K.; Huang, X.; Sagratini, G.; Silvi, S. Morpho-structural and chemical characterization of paper based materials with functionalized surface. *Mater. Chem. Phys.* **2021**, *267*, No. 124693.
(38) Thommes, M.; Kaneko, K.; Neimark, A. V.; Olivier, J. P.; Rodriguez-Reinoso, F.; Rouquerol, J.; Sing, K. S. W. Physisorption of gases, with special reference to the evaluation of surface area and pore size distribution (IUPAC Technical Report). *Pure Appl. Chem.* **2015**, *87*, 1051−1069.
(39) Bedane, A. H.; Xiao, H. N.; Eic, M.; Farmahini-Farahani, M. Structural and thermodynamic characterization of modified cellulose fiber-based materials and related interactions with water vapor. *Appl. Surf. Sci.* **2015**, *351*, 725−737.
(40) Ng, H. M.; Sin, L. T.; Bee, S. T.; Tee, T. T.; Rahmat, A. R. Review of Nanocellulose Polymer Composite Characteristics and Challenges. *Polym.-Plast. Technol. Eng.* **2017**, *56*, 687−731.
(41) Ali, M.; Chai, L.-Y.; Wang, H.-Y.; Tang, C.-J.; Min, X.-B.; Yan, X.; Peng, C.; Song, Y.-X.; Zheng, P. Enhanced short-cut nitrification in an airlift reactor by $CaCO_3$ attachment on biomass under high bicarbonate condition. *Biodegradation* **2016**, *27*, 131−144.
(42) Ali, M. A. M.; El-Nemr, K. F.; Hamada, A. A.; Abd-Elhady, W. S. Effect of gamma-irradiation on the mechanical behavior of EPDM rubber-recycled newsprint microfibers composites. *J. Vinyl Addit. Technol.* **2019**, *25*, 198−212.
(43) Akbarpour, I.; Ghasemian, A.; Resalati, H.; Saraeian, A. Biodeinking of mixed ONP and OMG waste papers with cellulase. *Cellulose* **2018**, *25*, 1265−1280.
(44) Wang, T.; Yang, H.; Kubicki, J. D.; Hong, M. Cellulose Structural Polymorphism in Plant Primary Cell Walls Investigated by High-Field 2D Solid-State NMR Spectroscopy and Density Functional Theory Calculations. *Biomacromolecules* **2016**, *17*, 2210−2222.
(45) De Silva, R.; Vongsanga, K.; Wang, X.; Byrne, N. Development of a novel regenerated cellulose composite material. *Carbohydr. Polym.* **2015**, *121*, 382−387.
(46) De Silva, R.; Wang, X.; Byrne, N. Tri-component bio-composite materials prepared using an eco-friendly processing route. *Cellulose* **2013**, *20*, 2461−2468.
(47) Fang, Z.; Li, B.; Liu, Y.; Zhu, J.; Li, G.; Hou, G.; Zhou, J.; Qiu, X. Critical Role of Degree of Polymerization of Cellulose in Super-Strong Nanocellulose Films. *Matter* **2020**, *2*, 1000−1014.
(48) Chen, Y.; Lee, H. V. Revalorization of selected municipal solid wastes as new precursors of ″green″ nanocellulose via a novel one-pot isolation system: A source perspective. *Int. J. Biol. Macromol.* **2018**, *107*, 78−92.
(49) Huang, J.; Liu, C.; Xie, L.; Zhang, R. Amorphous calcium carbonate: A precursor phase for aragonite in shell disease of the pearl oyster. *Biochem. Biophys. Res. Commun.* **2018**, *497*, 102−107.
(50) Chen, Y.; Jiang, Y.; Wan, J.; Wu, Q.; Wei, Z.; Ma, Y. Effects of wet-pressing induced fiber hornification on hydrogen bonds of cellulose and on properties of eucalyptus paper sheets. *Holzforschung* **2018**, *72*, 829−837.
(51) Altaner, C. M.; Thomas, L. H.; Fernandes, A. N.; Jarvis, M. C. How Cellulose Stretches: Synergism between Covalent and Hydrogen Bonding. *Biomacromolecules* **2014**, *15*, 791−798.
(52) Kondo, T. The assignment of IR absorption bands due to free hydroxyl groups in cellulose. *Cellulose* **1997**, *4*, 281−292.
(53) Moise, I. V.; Manea, M. M.; Vasilca, S.; Pintilie, C.; Virgolici, M.; Cutrubinis, M.; Stanculescu, I. R.; Meltzer, V. The crosslinking behaviour of cellulose in gamma irradiated paper. *Polym. Degrad. Stab.* **2019**, *160*, 53−59.
(54) Khandaker, S.; Chowdhury, M. F.; Awual, M. R.; Islam, A.; Kuba, T. Efficient cesium encapsulation from contaminated water by cellulosic biomass based activated wood charcoal. *Chemosphere* **2021**, *262*, No. 127801.
(55) Profili, J.; Asadollahi, S.; Vinchon, P.; Dorris, A.; Beck, S.; Sarkassian, A.; Stafford, L. Recent progress on organosilicon coatings deposited on bleached unrefined Kraft paper by non-thermal plasma process at atmospheric pressure. *Prog. Org. Coat.* **2020**, *147*, No. 105865.
(56) Gong, H.; Lin, X.; Xie, Y.; Liu, L.; Zhou, J.; Liao, H.; Shang, R.; Luo, X. A novel self-crosslinked gel microspheres of Premna microphylla turcz leaves for the absorption of uranium. *J. Hazard. Mater.* **2021**, *404*, No. 124151.
(57) Kasomo, R. M.; Li, H.; Zheng, H.; Chen, Q.; Weng, X.; Mwangi, A. D.; Ge, W.; Song, S. Selective flotation of rutile from almandine using sodium carboxymethyl cellulose (Na-CMC) as a depressant. *Miner. Eng.* **2020**, *157*, No. 106544.
(58) Deepa, B.; Abraham, E.; Cordeiro, N.; Mozetic, M.; Mathew, A. P.; Oksman, K.; Faria, M.; Thomas, S.; Pothan, L. A. Utilization of various lignocellulosic biomass for the production of nanocellulose: a comparative study. *Cellulose* **2015**, *22*, 1075−1090.
(59) Batuer, A.; Chen, D.; Yin, L.; Feng, Y. Correlation between mechanical properties and thermochemical behaviours of waste papers in their early devolatilization stage. *J. Anal. Appl. Pyrolysis* **2019**, *137*, 128−137.
(60) Tan, X.; Hamid, S. B. A.; Lai, C. W. Preparation of high crystallinity cellulose nanocrystals (CNCs) by ionic liquid solvolysis. *Biomass Bioenergy* **2015**, *81*, 584−591.
(61) Chirayil, C. J.; Joy, J.; Mathew, L.; Mozetic, M.; Koetz, J.; Thomas, S. Isolation and characterization of cellulose nanofibrils from Helicteres isora plant. *Ind. Crop. Prod.* **2014**, *59*, 27−34.
(62) Ji, Y.; Xu, Q.; Jin, L.; Fu, Y. Cellulosic paper with high antioxidative and barrier properties obtained through incorporation of tannin into kraft pulp fibers. *Int. J. Biol. Macromol.* **2020**, *162*, 678−684.
(63) Zhao, W.; Liang, Z.; Feng, Z.; Xue, B.; Xiong, C.; Duan, C.; Ni, Y. New Kind of Lignin/Polyhydroxyurethane Composite: Green Synthesis, Smart Properties, Promising Applications, and Good Reprocessability and Recyclability. *ACS Appl. Mater. Interfaces* **2021**, *13*, 28938−28948.


https://doi.org/10.1021/acsomega.3c01668
*ACS Omega* 2023, 8, 23673−23682